Biointerface Research in Applied Chemistry
Open-Access Journal (ISSN: 2069-5837)

Article
Volume 16, Issue 1, 2026, 10
https://doi.org/10.33263/BRIAC161.010

The Therapeutic Potential of *Moringa oleifera* in Inflammation-Induced Insulin Resistance: An Informatics Approach

Najib Najib [1,*], Turhadi Turhadi [1], Fatchiyah Fatchiyah [1,2,*]

[1] Department of Biology, Faculty of Mathematics and Natural Sciences, Brawijaya University, Malang, Indonesia; najib24@student.ub.ac.id (N.N.); turhadibioligi@ub.ac.id (T.T.); fatchiya@ub.ac.id (F.F.);
[2] Research Center of Smart Molecule of Natural Genetics Resources, Brawijaya University, Malang, Indonesia; fatchiya@ub.ac.id
* Correspondence: najib24@student.ub.ac.id (N.N.); fatchiya@ub.ac.id (F.F.);

Received: 4.10.2025; Accepted: 19.01.2026; Published: 15.02.2026

Abstract: Inflammation promotes insulin resistance by triggering the NF-κB signaling cascade, resulting in the production of pro-inflammatory cytokines like IL-6 and TNF-α. *Moringa oleifera* contains bioactive phytochemicals with reported anti-inflammatory potential, yet the molecular mechanisms underlying these effects remain unclear. This study aimed to identify novel drug targets for inflammation and to select a potent compound from M. oleifera with strong anti-inflammatory properties by suppressing the NF-κB cascade via *in silico* analysis. Phytochemicals of *M. oleifera* were screened for drug-likeness, toxicity, bioactivity, and membrane permeability. Target binding pockets in NF-κB, TNF-α, IL-6, and IKKβ were identified, followed by molecular docking and molecular dynamics (MD) simulations to evaluate binding affinity and complex stability. Four compounds met all screening criteria: quinic acid, kaempferol, 7-hydroxycoumarin, and p-coumaric acid. Kaempferol showed the strongest binding across all targets, with docking scores of -8.6, -8.5, -6.4, and -9.3 kcal/mol for NF-κB, TNF-α, IL-6, and IKKβ, respectively. Additionally, molecular dynamics analysis confirmed the stability of these interactions. These findings suggest that kaempferol can inhibit NF-κB signaling and its associated cytokines, offering a promising natural alternative for treating inflammation related to insulin resistance.

Keywords: anti-inflammatory; IKKβ; IL-6; informatics; insulin resistance; metabolic syndrome; *Moringa oleifera*; NF-κB; TNF-α.

1. Introduction

Inflammation is a complex biological response triggered by harmful stimuli, such as infections, injuries, or irritants. While it serves to eliminate harmful agents and initiate tissue repair, chronic or uncontrolled inflammation contributes to the pathogenesis of various diseases [1]. Metabolic Syndrome (MetS) is a multifactorial metabolic disorder that includes insulin resistance (IR), and chronic low-grade inflammation exacerbates its progression [2,3]. Adiposity is closely associated with the secretion of pro-inflammatory cytokines from adipose tissue, which further aggravate IR and promote the progression of MetS [4].

The nuclear factor kappa B (NF-κB) signaling cascade plays a pivotal role in linking inflammation to IR, by upregulating pro-inflammatory cytokines such as interleukin-6 (IL-6) and tumor necrosis factor-α (TNF-α), which impair insulin signaling [5]. NF-κB activation is primarily mediated by pro-inflammatory cytokines, including TNF-α, LPS, and IL-1. As a result, IκB is phosphorylated at serine, threonine, or tyrosine residues by IKK, leading to the degradation of IκB proteins that typically inhibit NF-κB activation. This degradation allows NF-κB dimers to move into the nucleus, where they activate the expression of genes involved in inflammation [6,7]. IL-6 and TNF-α impair insulin signaling by disrupting receptor function, thereby contributing to IR [8]. TNF-α further disrupts insulin signaling by promoting the serine phosphorylation of insulin receptor substrate proteins, creating a feedback loop that perpetuates both inflammation and IR [9]. This inflammatory environment is particularly pronounced in obesity, where excess fatty acids activate NF-κB signaling, leading to worsening metabolic dysregulation [10]. Given these associations, targeting inflammatory pathways such as NF-κB and IKKβ represents a promising therapeutic strategy to ameliorate IR. Interventions aimed at reducing inflammation, including anti-inflammatory agents, have been shown to improve metabolic parameters in patients with MetS [11]. These findings highlight the importance of addressing inflammation in the prevention and treatment of metabolic disorders.

Moringa oleifera, widely cultivated in tropical regions, has garnered attention for its anti-inflammatory properties and has traditionally been used in folk medicine to treat various inflammatory conditions [12]. This plant contains bioactive compounds, such as flavonoids, terpenoids, and isothiocyanates, which exhibit antioxidant and anti-inflammatory activities that help mitigate IR-associated inflammation [13-15]. Additionally, compounds such as kaempferol, quercetin, and rutin have demonstrated significant pharmacological effects, suggesting that *M. oleifera* may serve as a potential treatment for inflammation [16]. However, despite its recognized anti-inflammatory activity, the role of *M. oleifera* in ameliorating inflammation-induced IR, particularly through key pathways such as NF-κB, TNF-α, IL-6, and IKKβ, remains poorly defined. Identifying specific bioactive compounds with potent anti-inflammatory properties is essential for advancing drug development. This study employs an *in silico* approach to screen and identify bioactive compounds in M. oleifera with high potential to modulate inflammation-related targets, thereby providing insights into their possible therapeutic mechanisms for treating IR in MetS.

2. Materials and Methods

2.1. Identification of bioactive compounds in Moringa oleifera.

The bioactive compounds were selected based on a previous study that identified the major phytochemical constituents of *M. oleifera* leaves [17]. The SMILES (Simplified Molecular Input Line Entry System) representations of these compounds, intended for further analysis, were retrieved from the PubChem database (https://pubchem.ncbi.nlm.nih.gov/).

2.2. Evaluation of drug-like properties and toxicity.

The drug-like properties of *M. oleifera* bioactive compounds were assessed using the SwissADME web server (http://www.swissadme.ch/index.php) [18], based on Lipinski's rule of five, Veber's rule, and Egan's rule. Toxicity predictions, including the likelihood of toxicity induction and LD_{50} values, were analyzed for compounds that passed the drug-likeness screening using the ProTox web server (https://tox-new.charite.de/protox_II/) [19]. The

parameters used for organ and final toxicity were hepatoxicity, immunotoxicity, and cytotoxicity.

2.3. Bioactivity and membrane permeability screening.

The potential bioactivity of the screened compounds was evaluated using the PASS Online web server (https://www.way2drug.com/passonline/) [20], focusing on inflammation-related parameters. Permeability through biological membranes was evaluated using the PerMM web server, which calculates energy profiles and membrane-binding affinities based on the DOPC bilayer model, thereby allowing the identification of compounds with the potential to efficiently penetrate lipid membranes [21].

2.4. Target protein identification.

A literature search was conducted using the term " Inflammation related to Metabolic Syndrome (MetS), encompassing insulin resistance" as the search keyword. Based on the reviewed studies, NF-κB, TNF-α, IL-6, and IKKβ were identified as key mediators of inflammation that drive IR and related inflammatory disorders. To explore indirect protein interactions, the STRING 12.0 database (https://string-db.org/) was used, applying a high-confidence minimum interaction threshold of 0.7.

2.5. Protein-protein interaction network and functional annotation of target proteins.

The potential target proteins implicated in inflammation-driven insulin resistance—NF-κB, TNF-α, IL-6, and IKKβ—were analyzed for interactions using the STRING web server (https://string-db.org/) applying a high-confidence association score threshold of 0.7. Functional annotation of the target and interacting proteins was performed through Gene Ontology (GO) analysis using the SRPlot web server (https://www.bioinformatics.com.cn/en). GO classification categorizes proteins into three domains: biological processes, cellular components, and molecular functions.

2.6. Preparation of ligands.

The three-dimensional (3D) conformations of the compounds were obtained from the PubChem database (https://pubchem.ncbi.nlm.nih.gov/) in .sdf format. The protein PDB file was used to retrieve the TNF-α protein inhibitor [22]. Reference inhibitors, including dehydroxymethylepoxyquinomicin (DHMEQ) for NF-κB [23,24], clindamycin for IL-6 [25], and BMS-345541 for IKKβ [26] were downloaded from PubChem in .sdf format. All ligand structures were minimized and converted into a .pdb file using the Open Babel plugin with the PyRx 8.0 software [27].

2.7. Preparation of target proteins.

The 3D structures of the four target proteins— NF-κB, TNF-α, IL-6, and IKKβ —were sourced from the PDB database (https://www.rcsb.org/) (PDB ID: 1IKN, 6OP0, 1ALU, and 4KIK, respectively). The protein preparation procedure was performed using the Biovia Discovery Studio 2024 software (Dassault Systèmes Biovia, San Diego, California, USA) [28]. Afterward, water molecules and unnecessary groups were removed, and the structure

underwent geometry optimization and energy minimization. Protonation was subsequently applied using the Protonate 3D tool to generate the appropriate hydrogen configuration.

2.8. Predicting the active binding sites.

The active sites within the target proteins were determined using the Computed Atlas of Surface Topography of Proteins (CASTP) tool (http://cast.engr.uic.edu). This tool visualizes the binding pockets within the protein structures and identifies the amino acid residues present in each pocket [29]. The largest active binding sites, based on both surface area and volume, were identified for each protein listed in Table 1.

Table 1. Active binding site prediction of the target proteins using the CASTp tool.

Protein	Binding site (volume (SA) Å^3)	Surface area (area (SA) Å^2)
NF-κB	943.278	1133.582
TNF-α	1241.225	1385.615
IL-6	38.585	63.542
IKKβ	11924.739	3452.845

2.9. Molecular docking.

Docking simulations of the target proteins were performed using AutoDock Vina, integrated into PyRx 8.0 [30]. Ligands were loaded into PyRx 8.0 through the Add Ligand option,, while the prepared protein structures were imported using the Add Macromolecule option. After identifying the active-site residues, a docking grid was configured to enclose the corresponding binding region, as summarized in Table 2. Docking was performed using an exhaustiveness value of 8 and generating 9 binding modes as default Vina parameters. Ligand–protein docking was then performed, and the binding scores along with all docking output files were saved. The fusion of the docked ligand and the target protein was performed and saved in PDB format using PyMOL 3.1 software. The docking results were also visualized with Biovia Discovery Studio 2024 software (Dassault Systèmes Biovia, San Diego, California, USA) [31].

Table 2. Grid coordinates and predicted binding sites of the target proteins using CASTp.

Protein	PDB	Chain	Active sites	Grid coordinate (Å)	
				Center	Dimension
NF-kB	1IKN	A	20TYR, 21VAL, 22GLU, 23ILE, 24ILE, 26GLN, 29GLN, 30ARG, 49GLU, 79LYS, 80ASP, 81PRO, 83HIS, 141PHE, 158ARG, 175LEU, 176THR, 177PRO, 178VAL, 179LEU, 180SER, 181HIS, 182PRO, 184PHE, 218LYS, 219VAL, 220GLN, 221LYS, 222GLU, 241GLN, 242ALA, 244VAL, 245HIS, 246ARG, 247GLN, 248VAL.	X: 45.0408 Y: 24.1370 Z: 34.4171	**X: 39.7896** **Y: 33.6202** **Z: 29.0528**
		C	249LYS, 251VAL, 271ASP, 305ARG, 306GLN, 307PHE.		
		D	248TYR, 249GLN, 250GLY, 251TYR, 254TYR, 255GLN, 258TRP, 266GLN, 267GLN, 270GLY, 271GLN, 275GLU, 276ASN, 277LEU, 278GLN, 279MET, 280LEU, 281PRO, 282GLU, 283SER, 284GLU, 286GLU, 287GLU, 288SER, 289TYR, 290ASP, 291THR, 292GLU.		
TNF-α	6OP0	A	9SER, 11LYS, 13VAL, 57LEU. 59TYR, 61GLN, 75LEU, 94LEU, 95SER, 96ALA, 97ILE, 98LYS, 99SER, 100PRO, 101CYS, 102GLN, 114TRP, 115TYR, 116GLN, 117PRO, 118ILE, 119TYR, 120LUE, 121GLY, 123VAL, 155ILE, 156ALA, 157LEU.	X:-6.5557 Y:-1.9532 Z: 17.7694	**X: 55.8145** **Y: 57.6279** **Z: 55.1941**
		B	11LYS, 57LEU, 58ILE, 59TYR, 61GLN, 68GLY, 69CYS, 96ALA, 98LYS, 99SER, 100PRO, 101CYS, 112LYS, 113PRO, 114TRP, 115TYR, 116GLU, 117PRO, 118ILE, 119TYR, 120LEU, 121GLY, 122GLY, 155ILE, 156ALA, 157LEU.		
		C	11LYS, 13VAL, 57LEU, 59TYR, 60SER, 61GLN, 63LEU, 68GLY, 69CYS, 73HIS, 96ALA, 98LYS, 99SER, 100PRO, 101CYS, 112LYS, 113PRO, 114TRP, 115TYR, 116GLU,		

Protein	PDB	Chain	Active sites	Grid coordinate (Å)	
				Center	Dimension
			117PRO, 118ILE, 119TYR, 120LEU, 121GLY, 122GLY, 149GLN, 151TYR, 155ILE, 156ALA, 157LEU.		
IL-6	1ALU	A	95GLU,96VAL, 98LEU, 99GLU, 116GLN, 120LYS, 141PRO, 144ASN.	X: 10.1795 Y:-21.3040 Z: 16.4090	**X: 13.6122** **Y: 22.5127** **Z: 22.0653**
IKKβ	4KIK	A	9THR, 16GLU, 17MET, 18LYS, 19GLU, 20ARG, 21LEU, 22GLY, 23THR, 27GLY, 29VAL, 30ILE, 31ARG, 42ALA, 44LYS, 46CYS, 48GLN, 50LEU, 53ARG, 54ASN, 56GLU, 57ARG, 58TRP, 61GLU, 64ILE, 65MET, 74VAL, 94LEU, 96MET, 97GLU, 98TYR, 99CYS, 100GLN, 101GLY, 102GLY, 103ASP, 105ARG, 106LYS, 107TYR, 108LEU, 109ASN, 110GLN, 111PHE, 112GLU, 113ASN, 114CYS, 115CYS, 140ARG, 141ILE, 142ILE, 143HIS, 144ARG, 145ASP, 146LEU, 147LYS, 149GLU, 150ASN, 152VAL, 165ILE, 166ASP, 167LEU, 168GLY, 169TYR, 180THR, 181SER, 184GLY, 185THR, 187GLN, 188TYR, 189LEU, 197GLN, 198LYS, 199TYR, 200THR, 207SER, 214GLU, 217THR, 218GLY, 219PHE, 220ARG. 221PRO, 223LEU, 224PRO, 225ASN, 226TRP, 244VAL, 245VAL, 246SER, 247GLU, 248ASP, 249LEU, 250ASN, 254LYS, 256SER, 258SER, 260PRO, 261TYR, 262PRO, 407PRO, 408GLU, 409SER, 412CYS, 423PHE, 424PHE, 425GLN, 427ARG, 428LYS, 429VAL, 431GLY, 432GLN, 550SER, 558GLY, 562ASP, 565GLU, 571TYR, 572ARG, 573ARG, 575ARG, 576GLU, 577LYS, 578PRO, 579ARG, 582ARG.	X: 56.0220 Y: 18.8995 Z:-52.4777	**X: 51.8523** **Y: 71.5964** **Z: 41.8764**

Source: Computed Atlas of Surface Topography of Proteins (CASTP) (http://cast.engr.uic.edu)

2.10. Validation of docking protocol.

2.10.1. Redocking of co-crystallized ligand.

The docking protocol was validated by redocking the target proteins that had co-crystallized ligands. The procedure involved protein preparation, structural alignment, superimposition of the co-crystallized and redocked complexes, and calculation of the root mean square deviation (RMSD) [32]. Redocking was conducted using the same docking parameters applied to the test ligands, with the maximized grid box. The docking protocol was validated using the TNF-α, IL-6, and IKKβ proteins that co-crystallized with ligands. For the NF-κB protein, redocking could not be assessed because no co-crystallized ligand was available in the PDB.

2.10.2. Docking with decoy molecules.

Docking validation was carried out using decoy molecules from the ZINC database (https://zinc.docking.org/substances/home/), which were prepared and docked under identical settings as the active ligand. Binding scores of the decoys were compared against the active compound to evaluate the protocol's ability to distinguish active from inactive molecules. The docking protocol was considered valid when at least 80% of the decoys showed binding affinities that differentiated from the test ligand, following equation (1) [33].

$$(1)\ Decoy\ Percentage = \frac{\text{Total decoys with binding affinity higher/lower than ligand}}{\text{Total number of decoy}}\ \text{x } 100\%$$

2.11. Molecular dynamics (MD) simulations.

The stability of the protein-ligand complex interactions was assessed through molecular dynamics (MD) simulations (saved in PDB format). MD simulations were conducted using the YASARA (Yet Another Scientific Artificial Reality Application) (version 19.12.14) software, applying the AMBER14 force field [34]. The system was maintained under constant temperature (310 K), constant pressure (1 bar), pH 7.4, and a 0.9% salt concentration. Before the simulation, the complex was solvated using the TIP3P water model within a cubic box extending at least 10 Å from the protein surface, with the COSMO solvation model applied during charge assignment. A time-step of 2.5 fs was used with a multiple time-step scheme, and non-bonded interactions were calculated using a 12 Å cutoff [35]. After system preparation, a 20 ns MD simulation was performed under these conditions using kaempferol as the selected ligand. Protein stability was evaluated based on root mean square deviation (RMSD), RMSD of ligand movement, hydrogen bond (HB) formation, and root mean square fluctuation (RMSF), using the md_analyze macro program.

3. Results and Discussion

3.1. Assessment of drug-like properties, toxicity potential, and bioactivity.

The drug-likeness evaluation showed that 21 compounds met the criteria for Lipinski, Veber, and Egan parameters (Figure 1a).

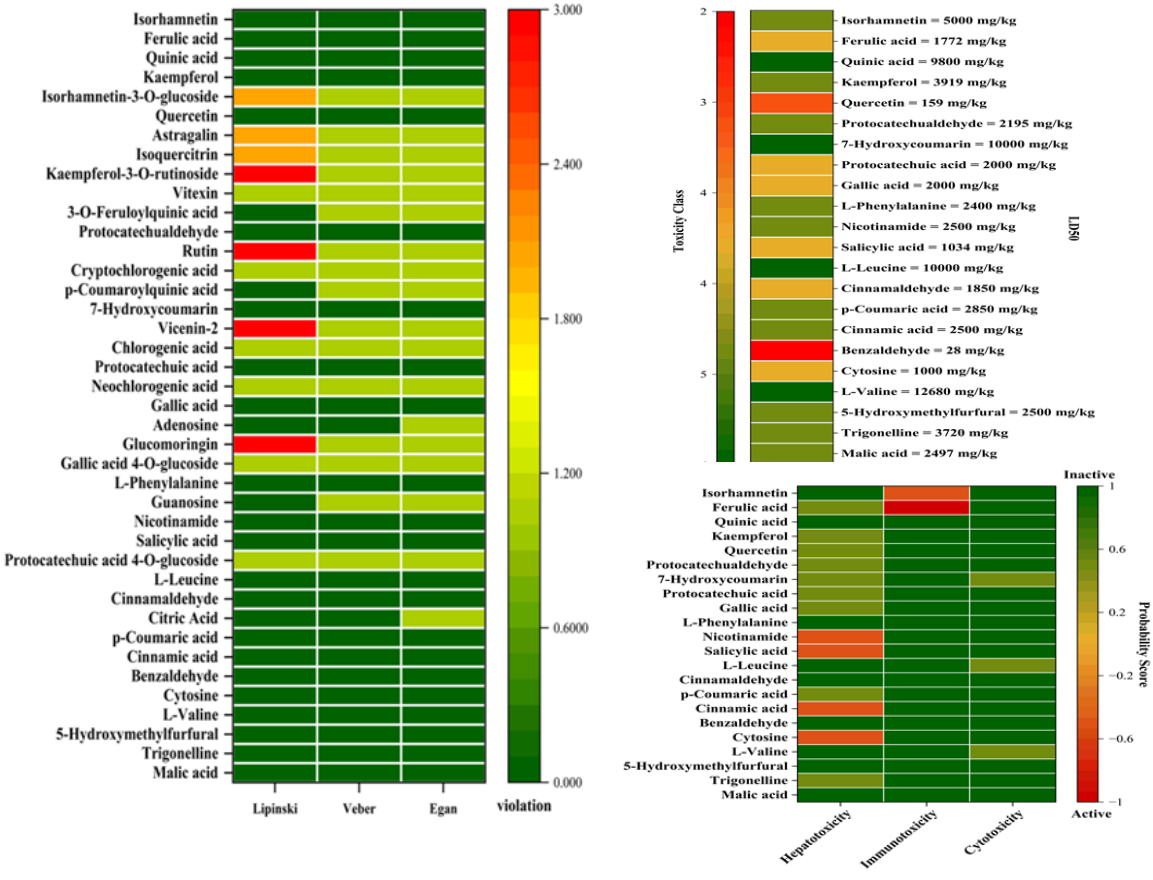

(a) **(b)**

Figure 1. Drug-likeness and toxicity screening of *M. oleifera* bioactive compounds**: (a)** drug-likeness screening using Lipinski, Veber, and Egan; **(b)** toxicity analysis according to LD_{50} and the probability of toxicity induction.

Subsequent toxicity screening identified 11 of these compounds as non-toxic to humans (Figure 1b). These 11 compounds then underwent bioactivity screening. Among them, quinic acid, kaempferol, 7-hydroxycoumarin, and p-coumaric acid showed the highest bioactivity potential across most inflammation-related parameters (Figure 2a). The four bioactive compounds were further evaluated for their ability to penetrate cell membranes. The findings revealed that all compounds were able to cross the plasma membrane (Figure 2b,c).

This study focused on predicting the compounds with the highest potential to combat inflammation associated with MetS, particularly in the context of IR. The results indicate that multiple metabolites from *M. oleifera* exhibit drug-like properties; however, through drug-likeness, toxicity, bioactivity, and membrane permeability screening, kaempferol emerged as the most promising candidate due to its superior pharmacokinetic properties and strong predicted anti-inflammatory potential. Kaempferol satisfied Lipinski, Veber, and Egan parameters, indicating it has drug-like properties. These parameters collectively reflect good blood solubility, efficient membrane permeability, and suitable metabolic and transport properties [36].

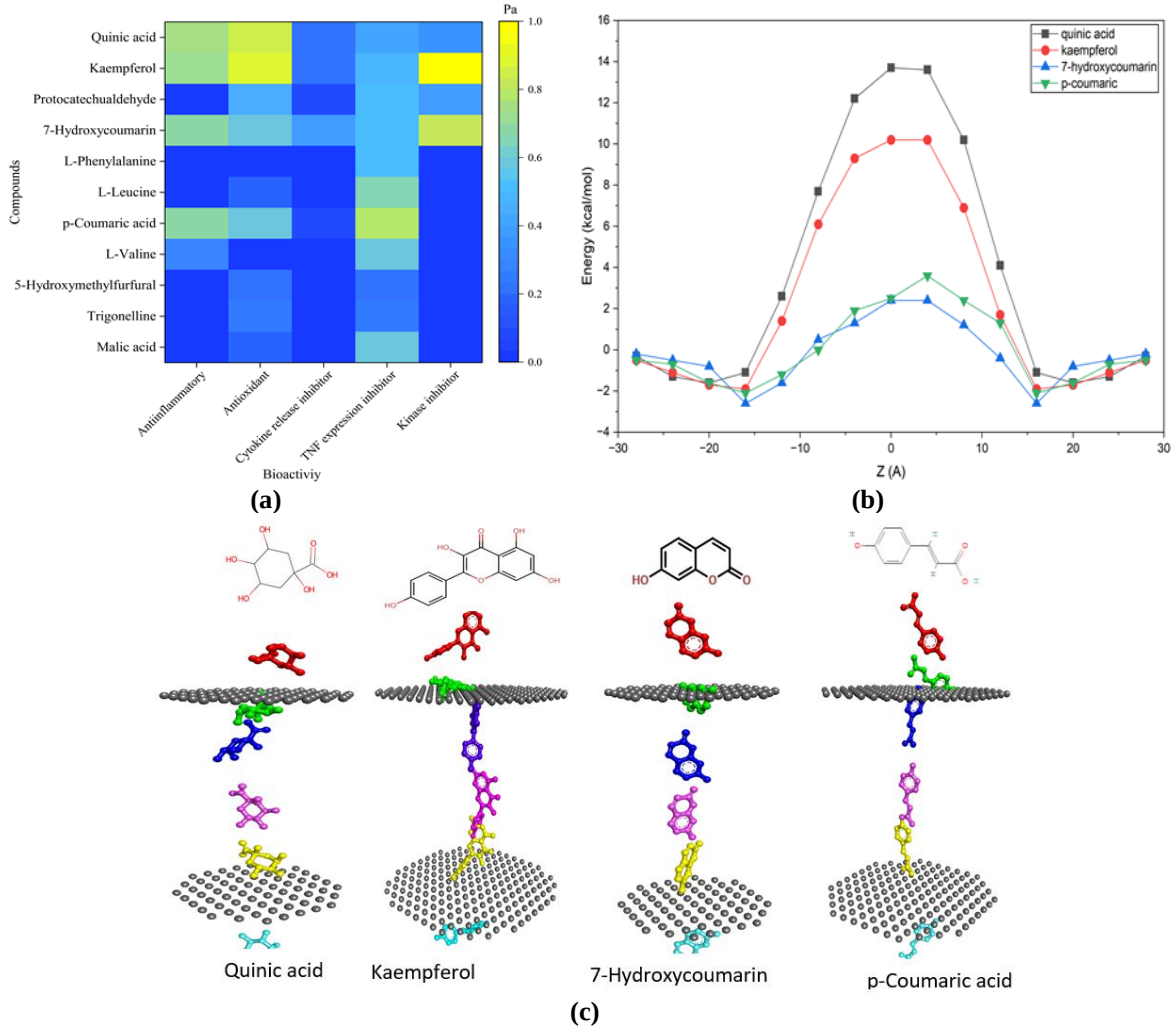

Figure 2. Bioactivity screening and membrane permeability of selected compounds: **(a)** bioactivity screening; **(b)** energy profiles of the four evaluated compounds during membrane permeation; **(c)** simulation of the penetration of quinic acid, kaempferol, 7-hydroxycoumarin, and p-coumaric acid through the lipid bilayer.

Toxicity evaluation using Pro-Tox predicted that kaempferol is non-toxic to humans. This tool applies a QSAR approach to evaluate compound toxicity, suggesting that kaempferol's structure does not resemble that of toxic compounds [19]. Moreover, PASS

Online analysis indicates that kaempferol has strong anti-inflammatory activity, with a Pa value above 0.8, suggesting a high probability of bioactivity. Higher Pa values reflect a stronger likelihood of the compound's specific bioactivity [20]. Kaempferol features a 3-hydroxyl group and 5,7-dihydroxy groups on its aromatic rings, with a planar three-ring structure, hydrophobic characteristics, and a C2–C3 double bond. This arrangement allows it to interact strongly with lipid bilayers and biological targets [37].

3.2. Target protein prediction and gene ontology (GO).

Protein interaction analysis using STRINGdb identified a complex network of key inflammatory proteins associated with IR, including NF-κB, TNF-α, IL-6, and IKKβ. These proteins form a complex network with several other proteins involved in inflammation and IR (Figure 3a).

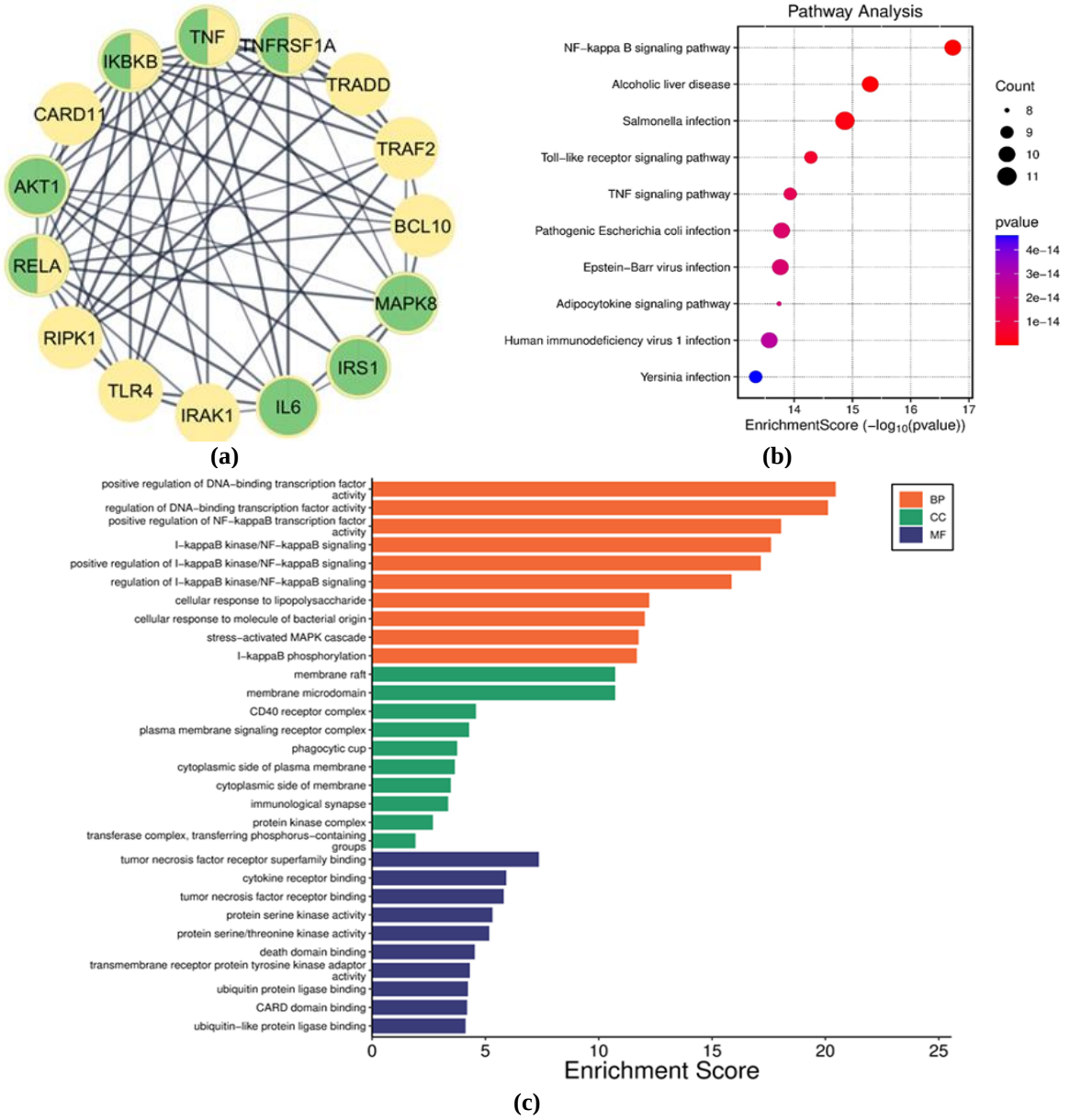

Figure 3. Protein-protein interaction network and functional annotation of target proteins for insulin resistance-related inflammation: NF-κB, TNF-α, IL-6, and IKKβ. **(a)** Protein-protein interaction. The yellow protein shows the NF-κB signaling pathway, the red protein shows the Proteins associated with insulin resistance; **(b)** gene ontology analysis; **(c)** biological process, cellular component, and molecular function analysis.

NF-κB (RELA) was found to form a network with several inflammation-related proteins, particularly those involved in the NF-κB signaling pathway (yellow nodes). NF-κB showed high-confidence interactions with 12 proteins. Among these, TNF-α, IL-6, and IKKβ exhibited the most complex interaction patterns, with multiple direct connections, reflecting their central roles in inflammation and IR. Proteins associated with IR (green nodes), such as IRS1 and AKT1, along with NF-κB, TNF-α, IL-6, and IKKβ, also showed strong interactions, indicating a close mechanistic relationship between chronic inflammation and impaired insulin signaling (Figure 3a). Gene ontology (GO) analysis revealed that NF-κB, IKKβ, TNF-α, and IL-6 were significantly involved and associated with the NF-κB signaling pathway (Figure 3b). These proteins operate synergistically within the NF-κB–mediated inflammatory response, predominantly localized in the cytoplasm and plasma membrane (Figure 3c).

This intricate network of inflammatory pathways contributes to IR in T2D by impairing insulin signaling and promoting chronic inflammation. The network is enriched with proteins involved in inflammatory responses, including the NF-κB pathway. NF-κB acts as a master transcriptional regulator of inflammatory genes, and its activation depends largely on IKKβ-mediated phosphorylation of IκB. This mechanism promotes nuclear translocation of NF-κB and induces the expression of cytokines such as TNF-α and IL-6, which further amplify inflammatory signaling [38-40]. TNF-α and IL-6 cytokines, in turn, activate the NF-κB pathway, amplifying inflammation and disrupting insulin signaling in key tissues, including the liver and muscles, thereby contributing to the onset of IR [41-43]. They play a pivotal role in the onset of IR by phosphorylating insulin receptor substrate-1 (IRS-1), thereby preventing its binding to the insulin receptor, reducing insulin signaling and uptake in metabolic tissues [44-46]. Inhibition of NF-κB, TNF-α, IL-6, and IKKβ would be expected to disrupt the NF-κB-driven inflammatory cascade, thereby decreasing downstream cytokine production. Targeting these proteins could provide potential therapeutic strategies for managing MetS and thereby alleviating chronic inflammation that contributes to impaired insulin signaling.

3.3. Structure retrieval and binding site identification.

Analysis of the binding pockets was performed using the CASTP server, as shown in Figure 4. The selected binding sites, along with their volumes and surface areas, are presented in Table 1 for further docking studies. The pocket's area and volume indicated its suitability for accommodating ligands of varying sizes.

3.4. Validation of docking.

Redocking of the co-crystallized ligands into the active sites of TNF-α, IL-6, and IKKβ was carried out using PyRx 0.8, following previously established procedures. The redocking step produced binding affinities of –8.7, –10.9, and –6.5 kcal/mol for TNF-α, IL-6, and IKKβ, respectively. The redocked complexes were then superimposed with their native protein–ligand complexes using PyMOL. The output files generated by PyRx 0.8 showed an RMSD of 0.00 Å between the native and redocked complexes. Additionally, the docking protocol employed allowed the co-crystallized ligands to bind to the same active site of the target protein after redocking (Figure 5). Decoy-based validation demonstrated that 12 out of 16 decoy molecules were correctly identified, yielding an 80% detection rate (Table 3).

The RMSD value of 0.00 Å between the co-crystallized ligand and redocked poses indicates that the docking protocol reproduced experimentally observed binding conformations

with precision. Such low RMSD values are desirable and are consistent with previous studies that have used the same redocking-based approach to validate docking protocols [47]. Furthermore, the close structural alignment between the redocked and co-crystallized ligand poses demonstrates that AutoDock Vina in PyRx 8.0 can accurately restore ligand positioning within the correct binding pockets of the target proteins [48]. The decoy screening further supports the scoring reliability of the docking workflow. Successfully identifying 80% of the decoys indicates that the algorithm can differentiate active ligands from non-binders, thereby strengthening confidence in subsequent virtual screening predictions [49].

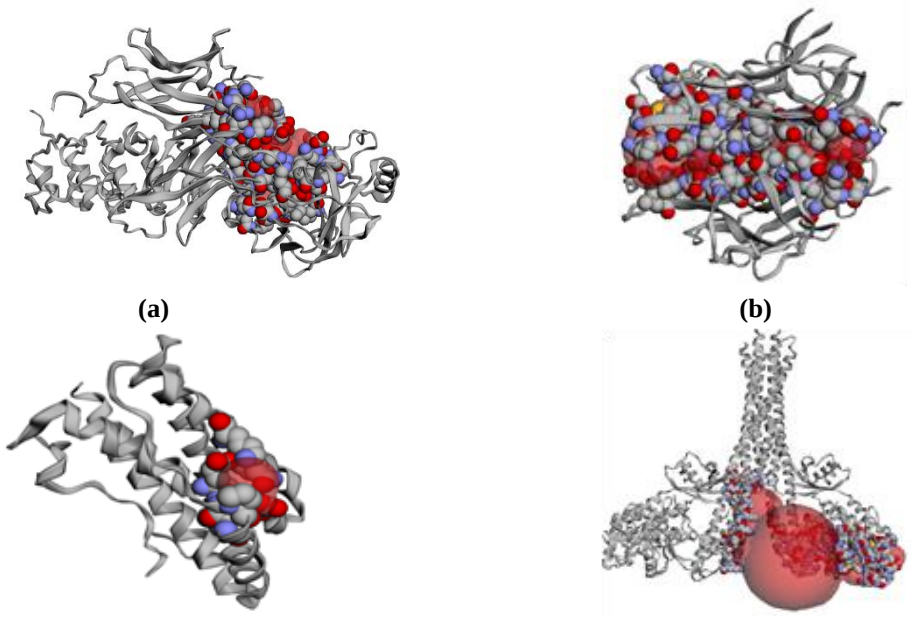

(a) **(b)** **(c)** **(d)**

Figure 4. Predicted binding pocket (highlighted) of the target protein using CASTp: **(a)** NF-kB (1IKN); **(b)** TNF-α (6OP0); **(c)** IL-6 (1ALU); **(d)** IKKβ (4KIK). These pockets were used as the docking sites for subsequent molecular docking and molecular dynamics simulations.

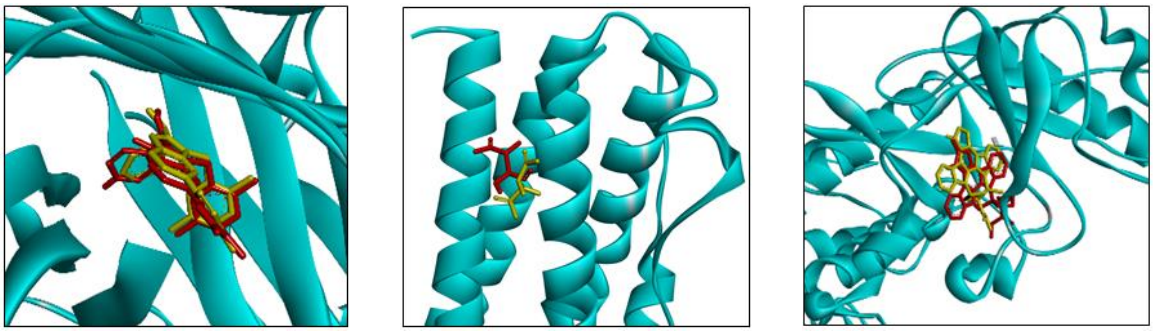

(a) **(b)** **(c)**

Figure 5. Superimposition of re-docked target proteins (red color) onto the original co-crystallized complex (yellow color) in the active site of the target proteins using the PyRx 0.8 tool. **(a)** TNF-α; **(b)** IL-6; **(c)** IKKβ.

Table 3. Validation of docking results of selected bioactive compounds from *M. oleifera* with decoys.

Protein	Test ligand	Binding affinity (kcal/mol)	Decoy ligands (kcal/mol)										Percentage (%)	Description
			1	2	3	4	5	6	7	8	9	10		
NF-κB	Quinic acid	-6.6	-5.8	-6.2	-6.8	-6.1	-6.2	-6.7	-5.5	-5.9	-6.0	-5.9	80	Moderate validity
	Kaempferol	-8.6	-7.7	-8.5	-8.3	-7.9	-7.8	-7.7	-8.3	-8.1	-8.4	-8.7	90	High validity
	7-hydroxycoumarin	-7.2	-6.1	-6.6	-7.3	-6.5	-6.2	-6.8	-7.0	-6.7	-6.4	-6.5	90	High validity
	p-coumaric acid	-6.7	-6.0	-5.5	-6.7	-6.3	-5.8	-5.9	-6.3	-6.1	-6.5	-6.8	80	Moderate validity

Protein	Test ligand	Binding affinity (kcal/mol)	Decoy ligands (kcal/mol)										Percentage (%)	Description
			1	2	3	4	5	6	7	8	9	10		
TNF-α	Quinic acid	-6.4	-6.3	-6.4	-6.4	-6.2	-6.3	-6.5	-6.2	-6.5	-6.4	-6.4	80	Moderate validity
	Kaempferol	-8.5	-8.3	-8.4	-8.0	-8.2	-8.3	-8.6	-8.7	-8.1	-8.4	-8.5	80	Moderate validity
	7-hydroxycoumarin	-7.6	-8.4	-7.7	-7.8	-8.0	-7.9	-8.9	-8.0	-7.1	-7.2	-7.9	80	Moderate validity
	p-coumaric acid	-7.6	-7.5	-7.6	-7.4	-7.3	-6.9	-7.3	-8.1	-7.2	-7.5	-6.5	90	High validity
IL-6	Quinic acid	-4.7	-4.6	-4.7	-4.7	-4.6	-4.8	-4.6	-4.7	-4.5	-4.6	-4.8	50	Low validity
	Kaempferol	-6.2	-6.0	-6.2	-5.9	-5.7	-6.2	-5.9	-6.4	-6.5	-6.1	-6.0	80	Moderate validity
	7-hydroxycoumarin	-4.7	-4.8	-4.5	-4.6	-4.6	-4.7	-4.9	-5.1	-4.5	-4.6	-4.6	70	Low validity
	p-coumaric acid	-4.7	-4.6	-4.4	-4.5	-4.4	-4.6	-4.8	-4.4	-4.6	-4.7	-4.6	80	Moderate validity
IKKβ	Quinic acid	-6.2	-6.0	-5.7	-6.2	-6.4	-6.1	-6.4	-6.2	-6.1	-5.8	-6.3	70	Low validity
	Kaempferol	-9.3	-9.3	-9.8	-9.8	-8.8	-9.9	-8.9	-9.7	-9.4	-9.5	-9.5	80	Moderate validity
	7-hydroxycoumarin	-7.0	-7.4	-7.0	-7.0	-7.2	-7.1	-8.1	-7.1	-6.7	-6.2	-7.3	80	Moderate validity
	p-coumaric acid	-6.7	-6.6	-7.4	-6.5	-6.7	-6.3	-6.8	-6.9	-6.5	-6.6	-6.1	70	Low validity

3.5. Binding interactions of bioactive compounds and target proteins.

Four selected compounds—quinic acid, kaempferol, 7-hydroxycoumarin, and p-coumaric acid—were further docked with each of NF-κB, TNF-α, IL-6, and IKKβ to evaluate their potential anti-inflammatory activity related to IR. The binding energies were -6.6, -8.6, -7.2, and -6.7 kcal/mol, respectively, with NF-κB; -6.4, -8.5, -7.6, and -7.6 kcal/mol, respectively, with TNF-α; -4.7, -6.2, -4.7, and -4.7 kcal/mol, respectively, with IL-6; and -7.2, -9.3, -7.0, and -6.7 kcal/mol, respectively, with IKKβ (Tables 3 and 4). According to the molecular docking results, kaempferol exhibited the lowest binding energy among all docked compounds and was therefore selected for subsequent *in silico* analyses, including molecular dynamics simulations. The docking results were similar to those of the reference NF-κB, TNF-α, IL-6, and IKKβ inhibitors, whose binding energies were -8.1, -13.6, -5.5, and -8.5 kcal/mol, respectively (Table 4). Additionally, kaempferol interacted with key protein residues within the active site, thereby supporting its strong binding affinity, as indicated by the residues highlighted in blue in Figure 6. The interactions between kaempferol and the target proteins, including hydrogen bonds and hydrophobic interactions, as well as the amino acids involved, are detailed in Table 4 and Figure 6.

Table 4. Chemical interactions of Kaempferol with NF-kB, TNF-α, IL-6, and IKK2.

Protein	Ligand	Binding affinity (kcal/mol)	Position of chemical interaction	
			Hydrogen bond	Hydrophobic interaction
NF-kB (PDB:1IKN)	Control	**-8.1**	GLY31, ASN186, ARG187, ALA188, THR191, ALA192, GLN220, SER276	
	Kaempferol	**-8.6**	ARG187, THR191, GLN220, ARG274, SER276	ARG30, ALA188, ALA192, ASP223
TNF-α (PDB: 6OP0)	Control	**-13.6**	TYR;A119, SER;C60, TYR;C151	LEU;A57, TYR; A59, LEU;B57, TYR;B59, TYR; B119, LEY;C57, TYR;C59, TYR;C119
	Kaempferol	**-8.5**	ILE;B58, TYR;C151	LEU;A57, LEU;B57, GLN;C61
IL-6 (PDB:1ALU)	Control	**-5.5**	GLU99, GLU95, LYS120, ASN144	LEU92, ILE123, PRO141

Protein	Ligand	Binding affinity (kcal/mol)	Position of chemical interaction	
			Hydrogen bond	Hydrophobic interaction
	Kaempferol	**-6.2**	GLN119, LYS120, PRO139, ASN144	GLU95, GLU99
IKKβ (PDB:4KIK)	Control	**-8.5**	LEU21, ASP103	VAL29, ALA42, VAL74, MET96, TYR98, VAL152, ILE165
	Kaempferol	**-9.3**	CYS99, ASP103, ASP166	LEU21, VAL29, ALA42, LYS44, MET96, VAL152, ILE165

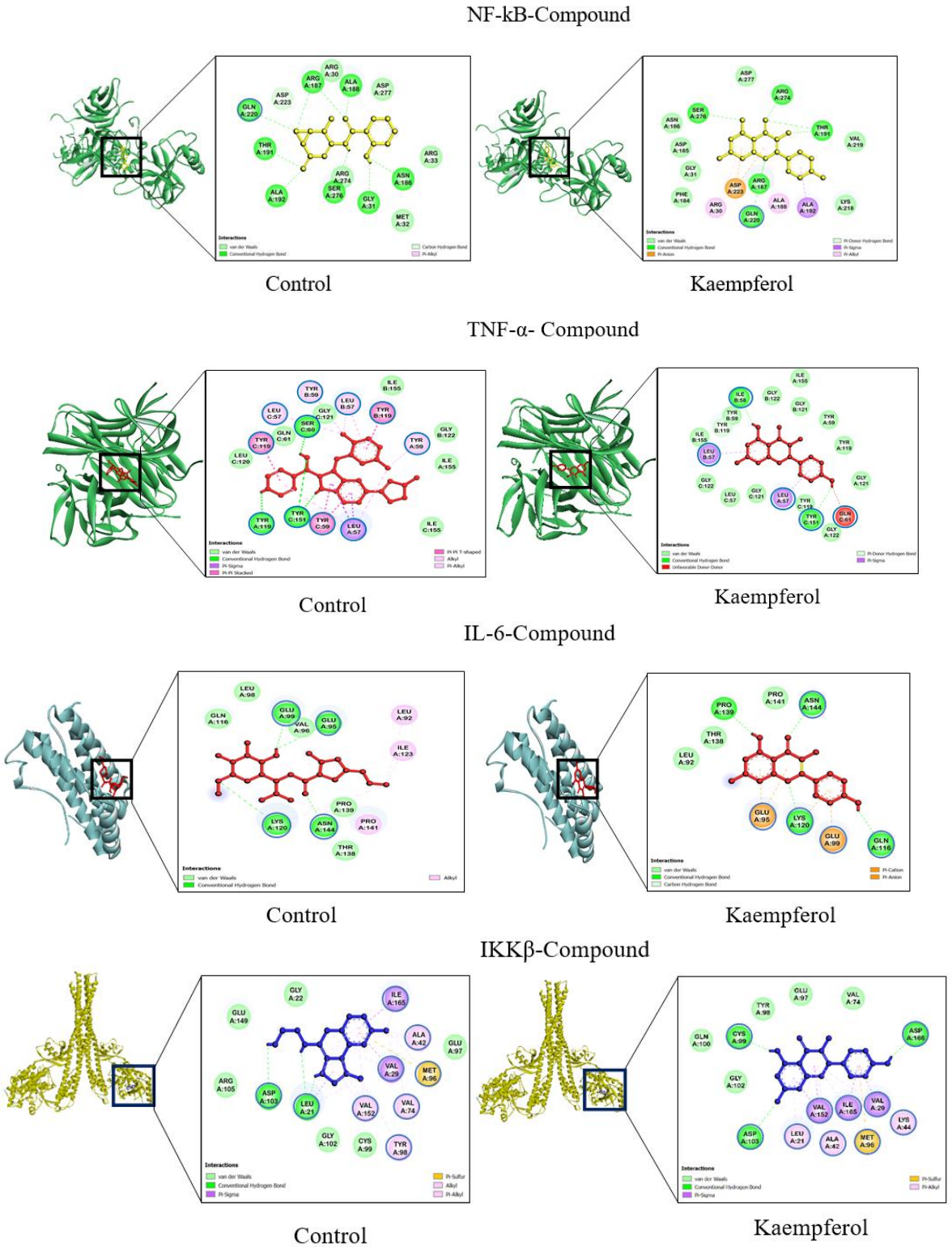

Figure 6. Molecular docking poses of kaempferol within the active sites of the target proteins, obtained using PyRx 8.0 software. Blue circles indicate key residues involved in ligand binding.

Based on the docking studies, kaempferol may act as a competitive inhibitor of the target proteins. Molecular docking results revealed that kaempferol bound to all four target proteins—NF-κB, TNF-α, IL-6, and IKKβ—at the same active sites occupied by their respective control ligands. In the NF-κB complex, kaempferol interacted within the same active pocket as the control ligand, forming a hydrogen bond with GLN220, as well as shared interacting residues including ARG187, ALA188, THR191, and ALA192. For the TNF-α protein, kaempferol established hydrogen bonds with ILE; B58 and TYR; C151, and hydrophobic interactions with LEU; A57, LEU; B57, and GLN; C61. These residues overlap with those engaged by the control ligand within the same active site region, indicating stable anchoring within the TNF-α binding pocket. Kaempferol also demonstrated strong binding to IL-6, forming four hydrogen bonds with GLN119, LYS120, PRO139, and ASN144, along with hydrophobic interactions with GLU95 and GLU99. These residues overlapped with those engaged by the control ligand, indicating that kaempferol occupied the same active-site region of IL-6. Among the four targets, the strongest interaction was observed with IKKβ, where kaempferol showed a binding affinity of −9.3 kcal/mol, surpassing that of the control ligand (−8.5 kcal/mol). Kaempferol interacted with several key active-site residues shared with the control, specifically ASP103, VAL29, MET96, VAL152, and ILE165.

These findings indicate that kaempferol consistently binds to the same functionally active sites as the control ligands across all target proteins, demonstrating high binding affinity and forming stabilizing interactions, highlighting its strong potential as a multi-target inhibitor within inflammatory signaling pathways. A high binding affinity indicates a robust protein-ligand interaction [50]. Kaempferol establishes hydrogen bonds that stabilize its interactions with the proteins [51]. Hydrogen bonds are essential for stabilizing protein structure and forming its secondary structure [52]. The presence of two intramolecular hydrogen bonds in kaempferol enhances its structural stability, and its high polarity ensures robust protein binding [53]. This unique structure contributes to kaempferol's diverse pharmacological activities, including its significant ability to suppress TNF-α expression in RAW cells stimulated with lipopolysaccharide [54].

3.6. Molecular dynamics (MD) simulation.

Molecular dynamics simulations were conducted to evaluate the stability of interactions between target proteins and kaempferol. A lower RMSD value indicates greater structural stability; protein–ligand complexes with RMSD values below 3 Å are considered to have stable interactions [55]. In this study, kaempferol was selected for MD simulations to evaluate its interactions with several inflammation-related target proteins over 20 ns. The molecular dynamics simulations indicated that kaempferol formed relatively stable complexes with NF-κB, TNF-α, and IL-6, as reflected by protein backbone RMSD values remaining below 3 Å (Figures 7a, 8a, and 9a). Meanwhile, the IKKβ-kaempferol complex is similarly stable to that of the IKKβ-inhibitor complex, but substantial fluctuations occurred as the simulation concluded (Figure 10a). Analysis of RMSD for ligand movement in the NF-κB-kaempferol complex revealed that kaempferol exhibited greater structural stability than the inhibitor throughout the simulation period (Figure 7b). The TNF-α-kaempferol complex showed an increase in RMSD at 2 ns, which then stabilized with minimal fluctuations until the end of the simulation (Figure 8b). While in IL-6 and IKKβ, kaempferol showed fluctuations at the end of the simulation (Figures 9b and 10b).

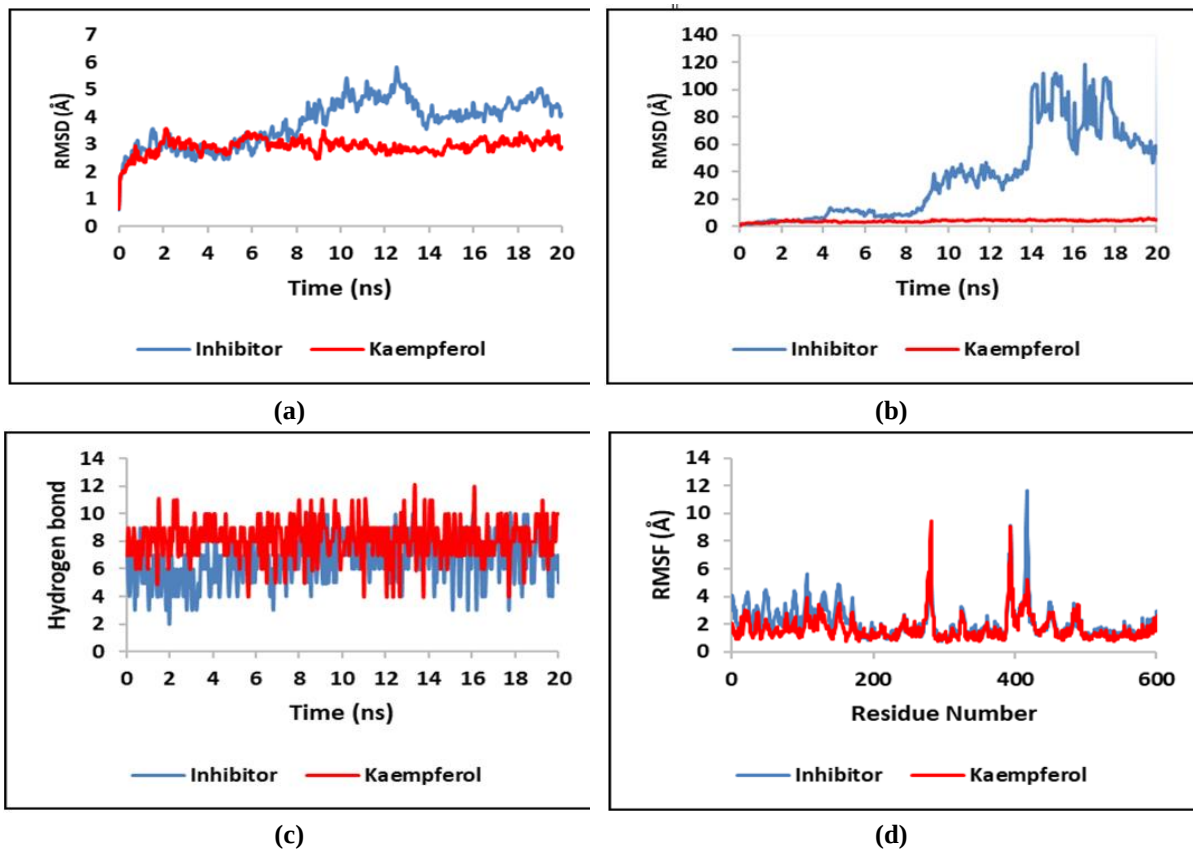

Figure 7. Molecular dynamic simulation of the interaction between NF-kB and the ligands: **(a)** RMSD; **(b)** RMSD ligand movement; **(c)** number of hydrogen bonds; **(d)** RMSF values.

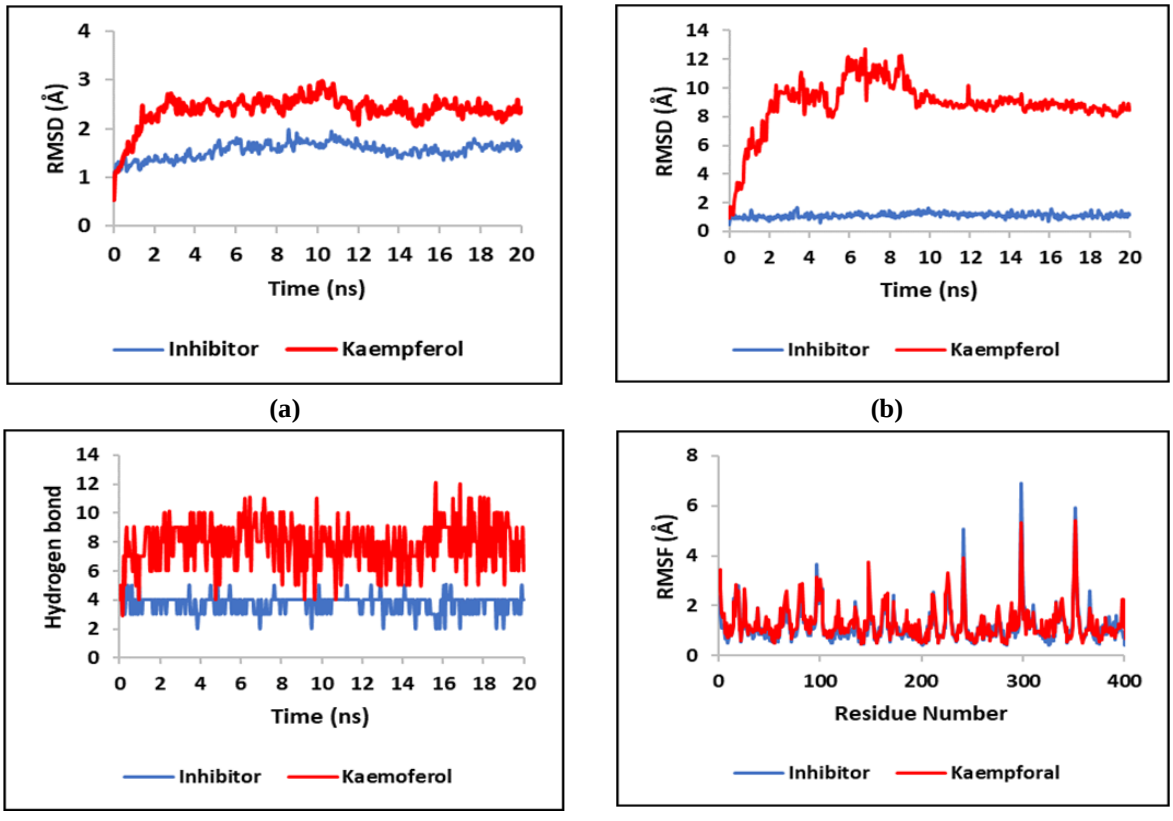

Figure 8. Molecular dynamic simulation of the interaction between TNF-α protein and the ligands: **(a)** RMSD; **(b)** RMSD ligand movement; **(c)** number of hydrogen bonds; **(d)** RMSF values.

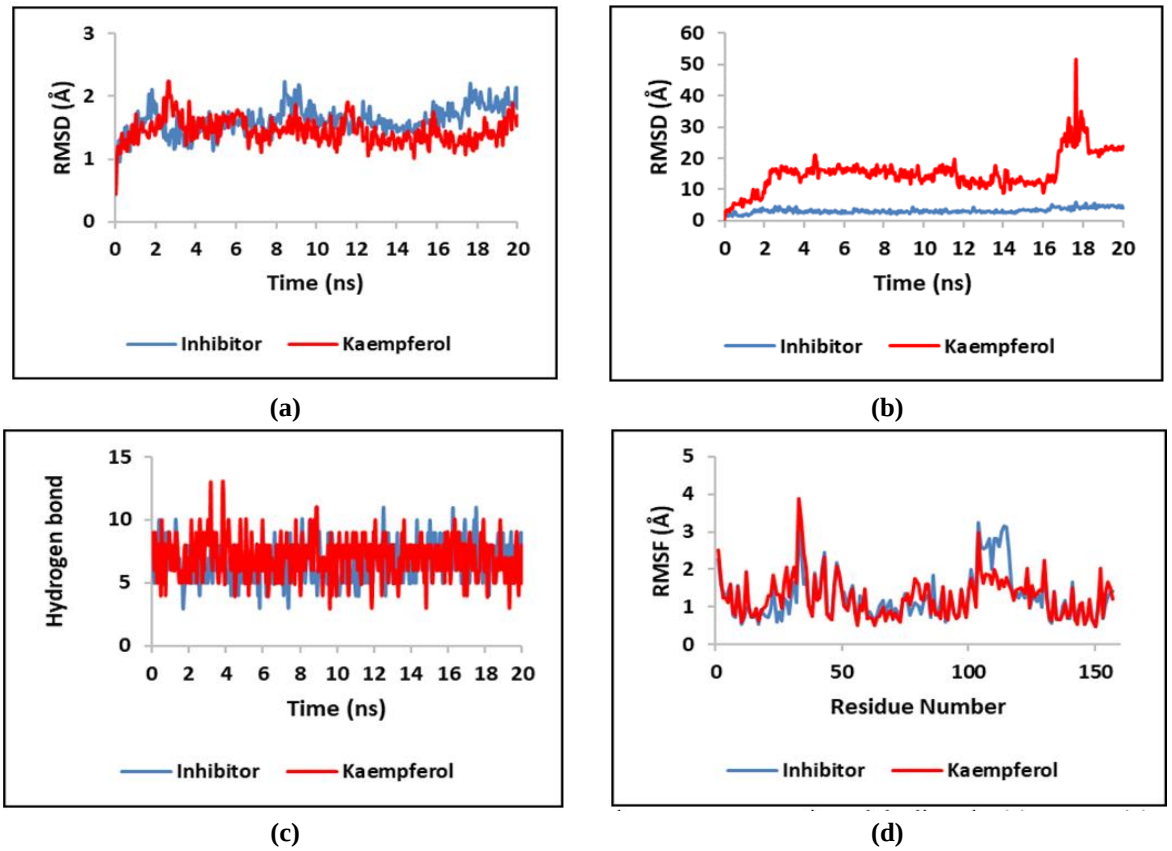

Figure 9. Molecular dynamic simulation of the interaction between IL-6 protein and the ligands: **(a)** RMSD; **(b)** RMSD ligand movement; **(c)** number of hydrogen bonds; **(d)** RMSF values.

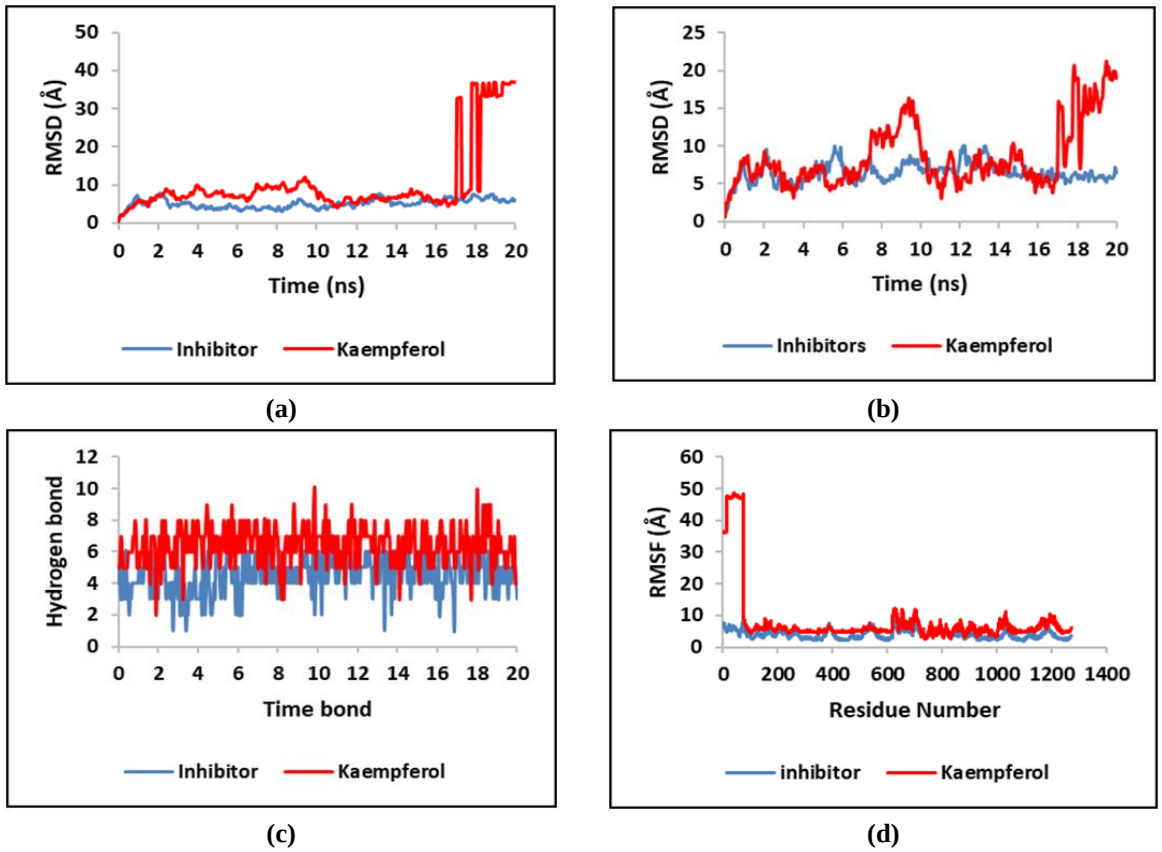

Figure 10. Molecular dynamic simulation of the interaction between IKKβ protein and the ligands: **(a)** RMSD; **(b)** RMSD ligand movement; **(c)** number of hydrogen bonds; (**d**) RMSF values.

In the hydrogen bond results, a greater number of hydrogen bonds were observed between NF-κB, TNF-α, and IKKβ with kaempferol than with the inhibitor (Figures 7c, 8c, and 10c). While in IL-6, the number of hydrogen bonds is the same as with the inhibitor (Figure 9c). RMSF analysis showed that the residue fluctuations of NF-κB, TNF-α, and IL-6 were comparable to those of the control (Figures 7a, 8a, and 9a). The RMSF values of IKKβ with kaempferol were found to be within the acceptable range, similar to those of the inhibitor, with only large fluctuations at the beginning of the simulation (Figure 10d). Overall, these results suggest that kaempferol maintains relatively more stable interactions with NF-κB, TNF-α, and IL-6 than with IKKβ over the simulation period, suggesting a possible role in modulating inflammatory pathways associated with IR.

Figure 11 presents a graphical abstract illustrating how the biological function of *M. oleifera* kaempferol may suppress pro-inflammatory cytokine expression, such as IL-6 and TNF-α, associated with the onset of IR. Kaempferol inhibits the NF-κB pathway, a major mediator of inflammation, thereby reducing pro-inflammatory cytokines [56,57]. By inhibiting these inflammatory markers, kaempferol may help restore insulin sensitivity, which is often compromised in individuals with MetS [58]. The current study highlights kaempferol's potential as a potent anti-inflammatory agent. However, the *in silico* findings should be validated in experimental models, both *in vitro* and *in vivo*. Establishing kaempferol as a treatment for inflammation and improving IR associated with MetS could represent a significant advancement in natural anti-inflammatory therapies.

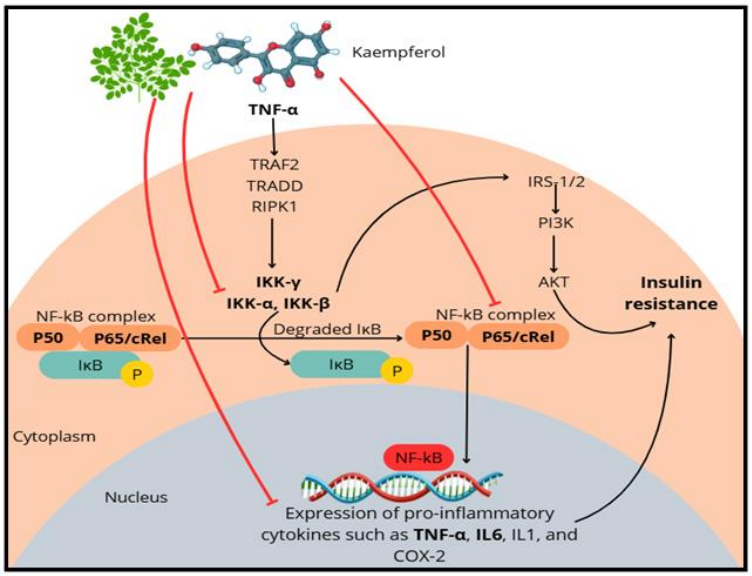

Figure 11. The possibility of the *Moringa kaempferol* biological function can inhibit proinflammatory cytokine expression, such as TNF-α and IL-6, contributing to ameliorating insulin resistance.

3.7. Limitations.

Molecular docking relies on scoring functions that provide approximate binding affinities and may not fully capture the dynamic nature of protein–ligand interactions. Additionally, the molecular dynamics simulations were conducted over a relatively short timescale (20 ns), which may be insufficient to fully assess the long-term stability of complex systems. Furthermore, the simulations were performed under simplified conditions that do not entirely represent the complexity of biological systems. Finally, the lack of experimental validation limits the extent to which the *in silico* findings can be generalized. Therefore, the results should be interpreted as preliminary and hypothesis-generating rather than conclusive.

4. Conclusions

This study presents a computational evaluation of selected bioactive compounds from M. oleifera and their interactions with inflammatory signaling proteins implicated in IR, namely NF-κB, TNF-α, IL-6, and IKKβ. The *in silico* analyses identified several compounds with favorable drug-likeness profiles, predicted non-toxicity, and stable binding interactions with the target proteins. Among the screened compounds, kaempferol exhibited stronger binding affinities and more stable interactions with key active-site residues, suggesting a potential capacity to modulate inflammatory signaling pathways associated with IR. However, as the findings are based exclusively on computational analyses, they are limited by methodological assumptions and require validation through *in vitro* and *in vivo* experiments. Accordingly, this study serves as a preliminary framework to support future experimental investigations.

Author Contributions

Conceptualization, N.N. and F.F.; methodology, N.N., F.F., and T.T.; software, N.N. and F.F.; validation, N.N., F.F., and T.T.; formal analysis, N.N.; investigation, F.F.; data curation, N.N. and F.F.; writing—original draft preparation, N.N.; writing—review and editing, N.N., F.F., and T.T.; supervision, F.F. and T.T. All authors have read and agreed to the published version of the manuscript.

Institutional Review Board Statement

Not applicable.

Informed Consent Statement

Not applicable.

Data Availability Statement

All data generated in this *in silico* study were obtained using publicly available computational tools, and the processed results are available from the corresponding author upon reasonable request.

Funding

None.

Acknowledgments

The authors appreciate the Bioinformatics course for providing facilities and guidance.

Conflicts of Interest

The authors confirm that they have no competing interests to disclose.

References

1. Dong, J. Signaling Pathways Implicated in Carbon Nanotube-Induced Lung Inflammation. *Front. Immunol.* **2020**, *11*, 552613, https://doi.org/10.3389/fimmu.2020.552613.
2. Wedell-Neergaard, A.-S.; Krogh-Madsen, R.; Petersen, G.L.; Hansen, Å.M.; Pedersen, B.K.; Lund, R.; Bruunsgaard, H. Cardiorespiratory fitness and the metabolic syndrome: Roles of inflammation and abdominal obesity. *PLOS ONE* **2018**, *13*, e0194991, https://doi.org/10.1371/journal.pone.0194991.
3. Sharma, P. Inflammation and the Metabolic Syndrome. *Indian J. Clin. Biochem.* **2011**, *26*, 317–318, https://doi.org/10.1007/s12291-011-0175-6.
4. Masenga, S.K.; Kabwe, L.S.; Chakulya, M.; Kirabo, A. Mechanisms of Oxidative Stress in Metabolic Syndrome. *Int. J. Mol. Sci.* **2023**, *24*, 7898, https://doi.org/10.3390/ijms24097898.
5. Pereira, S.S.; Alvarez-Leite, J.I. Low-Grade Inflammation, Obesity, and Diabetes. *Curr. Obes. Rep.* **2014**, *3*, 422–431, https://doi.org/10.1007/s13679-014-0124-9.
6. Zhao, W.M.; Qin, Y.L.; Niu, Z.P.; Chang, C.F.; Yang, J.; Li, M.H.; Zhou, Y.; Xu, C.S. Branches of the NF-κB signaling pathway regulate proliferation of oval cells in rat liver regeneration. *Genet. Mol. Res.* **2016**, *15*.
7. Zhang, Q.; Lenardo, M.J.; Baltimore, D. 30 Years of NF-κB: A Blossoming of Relevance to Human Pathobiology. *Cell* **2017**, *168*, 37-57, https://doi.org/10.1016/j.cell.2016.12.012.
8. Toshimitsu, T.; Gotou, A.; Sashihara, T.; Hachimura, S.; Shioya, N.; Suzuki, S.; Asami, Y. Effects of 12-Week Ingestion of Yogurt Containing *Lactobacillus plantarum* OLL2712 on Glucose Metabolism and Chronic Inflammation in Prediabetic Adults: A Randomized Placebo-Controlled Trial. *Nutrients* **2020**, *12*, 374, https://doi.org/10.3390/nu12020374.
9. Matsunaga, T.; Shoji, A.; Gu, N.; Joo, E.; Li, S.; Adachi, T.; Yamazaki, H.; Yasuda, K.; Kondoh, T.; Tsuda, K. γ-tocotrienol attenuates TNF-α-induced changes in secretion and gene expression of MCP-1, IL-6 and adiponectin in 3T3-L1 adipocytes. *Mol. Med. Rep.* **2012**, *5*, 905-909, https://doi.org/10.3892/mmr.2012.770.
10. Nisr, R.B.; Shah, D.S.; Ganley, I.G.; Hundal, H.S. Proinflammatory NFkB signalling promotes mitochondrial dysfunction in skeletal muscle in response to cellular fuel overloading. *Cell. Mol. Life Sci.* **2019**, *76*, 4887-4904, https://doi.org/10.1007/s00018-019-03148-8.
11. Montecucco, F.; Bertolotto, M.; Vuilleumier, N.; Franciosi, U.; Puddu, A.; Minetti, S.; Delrio, A.; Quercioli, A.; Bergamini, E.; Ottonello, L.; Pende, A.; Lenglet, S.; Pelli, G.; Mach, F.; Dallegri, F.; Viviani, G.L. Acipimox reduces circulating levels of insulin and associated neutrophilic inflammation in metabolic syndrome. *Am. J. Physiol. Endocrinol. Metab.* **2011**, *300*, E681-E690, https://doi.org/10.1152/ajpendo.00527.2010.
12. Fard, M.T.; Arulselvan, P.; Karthivashan, G.; Adam, S.K.; Fakurazi, S. Bioactive extract from Moringa oleifera inhibits the pro-inflammatory mediators in lipopolysaccharide stimulated macrophages. *Pharmacogn. Mag.* **2015**, *11*, S556, https://doi.org/10.4103/0973-1296.172961.
13. Mittal, A.; Sharma, M.; David, A.; Vishwakarma, P.; Saini, M.; Goel, M.; Saxena, K.K. An experimental study to evaluate the anti-inflammatory effect of moringa oleifera leaves in animal models. *Int. J. Basic Clin. Pharmacol.* **2017**, *6*, 452-457, https://doi.org/10.18203/2319-2003.ijbcp20170347.
14. Zainab, B.; Ayaz, Z.; Alwahibi, M.S.; Khan, S.; Rizwana, H.; Soliman, D.W.; Alawaad, A.; Mehmood Abbasi, A. *In silico* elucidation of *Moringa oleifera* phytochemicals against diabetes mellitus. *Saudi J. Biol. Sci.* **2020**, *27*, 2299-2307, https://doi.org/10.1016/j.sjbs.2020.04.002.
15. Pradana, D.L.C.; Rahmi, E.P.; Muti, A.F. Hypoglycemic effect of Moringa oleifera aqueous extract in diabetic animal studies: a mechanisms review. In Advances in Health Sciences Research, Proceedings of the 4th International Conference on Sustainable Innovation 2020–Health Science and Nursing (ICoSIHSN 2020), Yogyakarta, Indonesia, 13-14 October 2020; Wardaningsih, S.; Tamayo, M.D.B.; Thanee, S.; Natasom, A.; Poblete, M.-L.O.; Martin, N.M.; Naruse, K.; Nurumal, M.S.B., Eds.;
Atlantis Press: **2021**, Volume 33, pp. 619–623, https://doi.org/10.2991/ahsr.k.210115.117.
16. Rode, S.B.; Dadmal, A.; Salankar, H.V. Nature's Gold (Moringa Oleifera): Miracle Properties. *Cureus* **2022**, *14*, e26640, https://doi.org/10.7759/cureus.26640.
17. Wang, J.; Du, Y.; Jiang, L.; Li, J.; Yu, B.; Ren, C.; Yan, T.; Jia, Y.; He, B. LC-MS/MS-based chemical profiling of water extracts of *Moringa oleifera* leaves and pharmacokinetics of their major constituents in rat plasma. *Food Chem. X* **2024**, *23*, 101585, https://doi.org/10.1016/j.fochx.2024.101585.

18. Daina, A.; Michielin, O.; Zoete, V. SwissADME: a free web tool to evaluate pharmacokinetics, drug-likeness and medicinal chemistry friendliness of small molecules. *Sci. Rep.* **2017**, *7*, 42717, https://doi.org/10.1038/srep42717.
19. Banerjee, P.; Eckert, A.O.; Schrey, A.K.; Preissner, R. ProTox-II: a webserver for the prediction of toxicity of chemicals. *Nucleic Acids Res.* **2018**, *46*, W257-W263, https://doi.org/10.1093/nar/gky318.
20. Filimonov, D.A.; Lagunin, A.A.; Gloriozova, T.A.; Rudik, A.V.; Druzhilovskii, D.S.; Pogodin, P.V.; Poroikov, V.V. Prediction of the Biological Activity Spectra of Organic Compounds Using the Pass Online Web Resource. *Chem. Heterocycl. Compd.* **2014**, *50*, 444-457, https://doi.org/10.1007/s10593-014-1496-1.
21. Lomize, A.L.; Hage, J.M.; Schnitzer, K.; Golobokov, K.; LaFaive, M.B.; Forsyth, A.C.; Pogozheva, I.D. PerMM: A Web Tool and Database for Analysis of Passive Membrane Permeability and Translocation Pathways of Bioactive Molecules. *J. Chem. Inf. Model.* **2019**, *59*, 3094-3099, https://doi.org/10.1021/acs.jcim.9b00225.
22. Arora, S.; Rushiya, P.; Tirpude, K.; Sapkal, N.; Yende, S.; Ittadwar, A.; Shah, S. Exploring the phytoconstituents targeting TNF-α as potential lead compounds to treat inflammatory diseases: an *in silico* approach. *Digit. Chin. Med.* **2022**, *5*, 264-275, https://doi.org/10.1016/j.dcmed.2022.10.003.
23. Ma, J.; Zhang, Y.; Sugai, T.; Kubota, T.; Keino, H.; El-Salhy, M.; Ozaki, M.; Umezawa, K. Inhibition of Cellular and Animal Inflammatory Disease Models by NF-κB Inhibitor DHMEQ. *Cells* **2021**, *10*, 2271, https://doi.org/10.3390/cells10092271.
24. Kanan, T.; Kanan, D.; Erol, I.; Yazdi, S.; Stein, M.; Durdagi, S. Targeting the NF-κB/IκBα complex via fragment-based E-Pharmacophore virtual screening and binary QSAR models. *J. Mol. Graph. Model.* **2019**, *86*, 264-277, https://doi.org/10.1016/j.jmgm.2018.09.014.
25. Forid, M.S.; Patil, R.B.; Roney, M.; Huq, A.K.M.M.; Mohd Nasir, M.H.B.; Mohd Aluwi, M.F.F.; Azuri, M.S.; Wan Ishak, W.M.B. Identification of β-cycloidal-derived mono-carbonyl curcumin analogs as potential interleukin-6 inhibitor to treat wound healing through QSAR, molecular docking, MD simulation, MM-GBSA calculation. *J. Biomol. Struct. Dyn.* **2025**, *43*, 8550-8561, https://doi.org/10.1080/07391102.2024.2331089.
26. Tian, F.; Zhou, P.; Kang, W.; Luo, L.; Fan, X.; Yan, J.; Liang, H. The small-molecule inhibitor selectivity between IKK*α* and IKK*β* kinases in NF-κB signaling pathway. *Recept. Signal Transduct. Res.* **2015**, *35*, 307-318, https://doi.org/10.3109/10799893.2014.980950.
27. O'Boyle, N.M.; Banck, M.; James, C.A.; Morley, C.; Vandermeersch, T.; Hutchison, G.R. Open Babel: An open chemical toolbox. *J. Cheminform.* **2011**, *3*, 33, https://doi.org/10.1186/1758-2946-3-33.
28. Fatchiyah, F.; Umar, J.f.; Turhadi, T.; Suyanto, E.; Wihastuti, T.A. Computational screening of the potent bioactive compound of brown rice (Oryza sativa L.) against obesityrelated hypercholesterolemia by targeting FASN, HMGCS1, and HMGCR. *J. Res. Pharm. Pract.* **2025**, *29*, 2486-2507, https://doi.org/10.12991/jrespharm.1798014.
29. Tian, W.; Chen, C.; Lei, X.; Zhao, J.; Liang, J. CASTp 3.0: computed atlas of surface topography of proteins. *Nucleic Acids Res.* **2018**, *46*, W363-W367, https://doi.org/10.1093/nar/gky473.
30. Trott, O.; Olson, A.J. AutoDock Vina: Improving the speed and accuracy of docking with a new scoring function, efficient optimization, and multithreading. *J. Comput. Chem.* **2010**, *31*, 455-461, https://doi.org/10.1002/jcc.
31. Agnihotri, P.; Deka, H.; Chakraborty, D.; Monu; Saquib, M.; Kumar, U.; Biswas, S. Anti-inflammatory potential of selective small compounds by targeting TNF-α & NF-kB signaling: a comprehensive molecular docking and simulation study. *J. Biomol. Struct. Dyn.* **2023**, *41*, 13815-13828, https://doi.org/10.1080/07391102.2023.2196692.
32. Shivanika, C.; Deepak Kumar, S.; Ragunathan, V.; Tiwari, P.; Sumitha, A.; Brindha Devi, P. Molecular docking, validation, dynamics simulations, and pharmacokinetic prediction of natural compounds against the SARS-CoV-2 main-protease. *J. Biomol. Struct. Dyn.* **2022**, 40, 585-611, https://doi.org/10.1080/07391102.2020.1815584.
33. Chaput, L.; Martinez-Sanz, J.; Quiniou, E.; Rigolet, P.; Saettel, N.; Mouawad, L. vSDC: a method to improve early recognition in virtual screening when limited experimental resources are available. *J. Cheminform.* **2016**, *8*, 1, https://doi.org/10.1186/s13321-016-0112-z.
34. Krieger, E.; Vriend, G. YASARA View—molecular graphics for all devices—from smartphones to workstations. *Bioinformatics* **2014**, *30*, 2981–2982, https://doi.org/10.1093/bioinformatics/btu426.

35. Dash, R.; Junaid, M.; Mitra, S.; Arifuzzaman, M.; Hosen, S.M.Z. Structure-based identification of potent VEGFR-2 inhibitors from *in vivo* metabolites of a herbal ingredient. *J. Mol. Model.* **2019**, *25*, 98, https://doi.org/10.1007/s00894-019-3979-6.
36. Bickerton, G.R.; Paolini, G.V.; Besnard, J.; Muresan, S.; Hopkins, A.L. Quantifying the chemical beauty of drugs. *Nat. Chem.* **2012**, *4*, 90-98, https://doi.org/10.1038/nchem.1243.
37. Ulrih, N.P.; Maričić, M.; Ota, A.; Šentjurc, M.; Abram, V. Kaempferol and quercetin interactions with model lipid membranes. *Food Res. Int.* **2015**, *71*, 146-154, https://doi.org/10.1016/j.foodres.2015.02.029.
38. Welty, F.K.; Alfaddagh, A.; Elajami, T.K. Targeting inflammation in metabolic syndrome. *Transl. Res.* **2016**, *167*, 257-280, https://doi.org/10.1016/j.trsl.2015.06.017.
39. Serasanambati, M.; Chilakapati, S.R. Function of Nuclear Factor Kappa B (NF-kB) in human diseases- A Review. *South Indian J. Biol. Sci.* **2016**, *2*, 368-387.
40. Liu, M.; Sakamaki, T.; Casimiro, M.C.; Willmarth, N.E.; Quong, A.A.; Ju, X.; Ojeifo, J.; Jiao, X.; Yeow, W.-S.; Katiyar, S.; Shirley, L.A.; Joyce, D.; Lisanti, M.P.; Albanese, C.; Pestell, R.G. The Canonical NF-κB Pathway Governs Mammary Tumorigenesis in Transgenic Mice and Tumor Stem Cell Expansion. *Cancer Res.* **2010**, *70*, 10464-10473, https://doi.org/10.1158/0008-5472.CAN-10-0732.
41. Esser, N.; Legrand-Poels, S.; Piette, J.; Scheen, A.J.; Paquot, N. Inflammation as a link between obesity, metabolic syndrome and type 2 diabetes. *Diabetes Res. Clin. Pract.* **2014**, *105*, 141-150, https://doi.org/10.1016/j.diabres.2014.04.006.
42. Benzler, J.; Ganjam, G.K.; Pretz, D.; Oelkrug, R.; Koch, C.E.; Legler, K.; Stöhr, S.; Culmsee, C.; Williams, L.M.; Tups, A. Central Inhibition of IKKβ/NF-κB Signaling Attenuates High-Fat Diet–Induced Obesity and Glucose Intolerance. *Diabetes* **2015**, *64*, 2015-2027, https://doi.org/10.2337/db14-0093.
43. Saltiel, A.R.; Olefsky, J.M. Inflammatory mechanisms linking obesity and metabolic disease. *J. Clin. Invest.* **2017**, *127*, 1–4, https://doi.org/10.1172/JCI92035.
44. Alipourfard, I.; Datukishvili, N.; Mikeladze, D. TNF-α Downregulation Modifies Insulin Receptor Substrate 1 (IRS-1) in Metabolic Signaling of Diabetic Insulin-Resistant Hepatocytes. *Mediators Inflamm.* **2019**, *2019*, 3560819, https://doi.org/10.1155/2019/3560819.
45. Zheng, X.; Ke, Y.; Feng, A.; Yuan, P.; Zhou, J.; Yu, Y.; Wang, X.; Feng, W. The Mechanism by Which Amentoflavone Improves Insulin Resistance in HepG2 Cells. *Molecules* **2016**, *21*, 624, https://doi.org/10.3390/molecules21050624.
46. Li, Z.; Kim, H.J.; Park, M.S.; Ji, G.E. Effects of fermented ginseng root and ginseng berry on obesity and lipid metabolism in mice fed a high-fat diet. *J. Ginseng Res.* **2018**, *42*, 312-319, https://doi.org/10.1016/j.jgr.2017.04.001.
47. Zothantluanga, J.H.; Aswin, S.K.; Rudrapal, M.; Cheita, D. Antimalarial Flavonoid-Glycoside from Acacia pennata with Inhibitory Potential Against *Pf*DHFR-TS: An *In silico* Study. *Biointerface Res. Appl. Chem.* **2022**, *12*, 4871–4887, https://doi.org/10.33263/BRIAC124.48714887.
48. Etsassala, N.G.E.R.; Badmus, J.A.; Marnewick, J.L.; Iwuoha, E.I.; Nchu, F.; Hussein, A.A. Alpha-Glucosidase and Alpha-Amylase Inhibitory Activities, Molecular Docking, and Antioxidant Capacities of *Salvia aurita* Constituents. *Antioxidants* **2020**, *9*, 1149, https://doi.org/10.3390/antiox9111149.
49. Vieira, T.F.; Sousa, S.F. Comparing AutoDock and Vina in Ligand/Decoy Discrimination for Virtual Screening. *Appl. Sci.* **2019**, *9*, 4538, https://doi.org/10.3390/app9214538.
50. Pantsar, T.; Poso, A. Binding Affinity via Docking: Fact and Fiction. *Molecules* **2018**, *23*, 1899, https://doi.org/10.3390/molecules23081899.
51. Majewski, M.; Ruiz-Carmona, S.; Barril, X. An investigation of structural stability in protein-ligand complexes reveals the balance between order and disorder. *Commun. Chem.* **2019**, *2*, 110, https://doi.org/10.1038/s42004-019-0205-5.
52. Pace, C.N.; Fu, H.; Lee Fryar, K.; Landua, J.; Trevino, S.R.; Schell, D.; Thurlkill, R.L.; Imura, S.; Scholtz, J.M.; Gajiwala, K.; Sevcik, J.; Urbanikova, L.; Myers, J.K.; Takano, K.; Hebert, E.J.; Shirley, B.A.; Grimsley, G.R. Contribution of hydrogen bonds to protein stability. *Protein Sci.* **2014**, *23*, 652-661, https://doi.org/10.1002/pro.2449.
53. Milenković, D.; Dimitrić Marković, J.M.; Dimić, D.; Jeremić, S.; Amić, D.; Stanojević Pirković, M.; Marković, Z.S. Structural characterization of kaempferol: a spectroscopic and computational study. *Maced. J. Chem. Chem. Eng.* **2019**, *38*, 49-62, https://doi.org/10.20450/mjcce.2019.1333.
54. Hung, T.M.; Dang, N.H.; Kim, J.C.; Choi, J.S.; Lee, H.K.; Min, B.-S. Phenolic glycosides from *Alangium salviifolium* leaves with inhibitory activity on LPS-induced NO, PGE_2, and TNF-α production. *Bioorg. Med. Chem. Lett.* **2009**, *19*, 4389-4393, https://doi.org/10.1016/j.bmcl.2009.05.070.

55. Widyananda, M.H.; Wicaksono, S.T.; Rahmawati, K.; Puspitarini, S.; Ulfa, S.M.; Jatmiko, Y.D.; Masruri, M.; Widodo, N. A Potential Anticancer Mechanism of Finger Root (Boesenbergia rotunda) Extracts against a Breast Cancer Cell Line. *Scientifica* **2022**, *2022*, 9130252, https://doi.org/10.1155/2022/9130252.
56. Suchal, K.; Malik, S.; Khan, S.I.; Malhotra, R.K.; Goyal, S.N.; Bhatia, J.; Ojha, S.; Arya, D.S. Molecular Pathways Involved in the Amelioration of Myocardial Injury in Diabetic Rats by Kaempferol. *Int. J. Mol. Sci.* **2017**, *18*, 1001, https://doi.org/10.3390/ijms18051001.
57. Naz, R.; Saqib, F.; Awadallah, S.; Wahid, M.; Latif, M.F.; Iqbal, I.; Mubarak, M.S. Food Polyphenols and Type II Diabetes Mellitus: Pharmacology and Mechanisms. *Molecules* **2023**, *28*, 3996, https://doi.org/10.3390/molecules28103996.
58. Deka, H.; Choudhury, A.; Dey, B.K. An Overview on Plant Derived Phenolic Compounds and Their Role in Treatment and Management of Diabetes. *J. Pharmacopuncture* **2022**, *25*, 199–208, https://doi.org/10.3831/KPI.2022.25.3.199.

Publisher's Note & Disclaimer